The RNA binding protein IMP1/ZBP1 drives mRNA local translation in microglia and mediates polarized migration and phagocytosis in response to inflammation.

Running title: Local protein synthesis in microglia.

Keywords: mRNA localization, local protein synthesis, microglia, RNA binding protein IMP1/ZBP1, inflammation

Josune Imaz-Iruretagoyena[1,2]*, Maite Blanco-Urrejola[1,2,3]*, Aida de la Cruz-Gambra[1,2], Mar Márquez[1,2], Amanda Sierra[1,4,5] and Jimena Baleriola[1,4,†].

[1] Achucarro Basque Center for Neuroscience, 48940 Leioa, Spain.

[2] Departamento de Neurociencias, Universidad del País Vasco (UPV/EHU), 48940 Leioa, Spain.

[3] Departamento de Biología Celular e Histología, Universidad del País Vasco (UPV/EHU), 48940 Leioa, Spain.

[4] IKERBASQUE, Basque Foundation for Science, 48009 Bilbao, Spain.

[5] Departamento de Bioquímica y Biología Molecular, Universidad del País Vasco (UPV/EHU), 48940 Leioa, Spain.

* These authors contributed equally to this work.

[†] Correspondence: Dr. Jimena Baleriola (jimena.baleriola@achucarro.org).

ABSTRACT

Polarized cells in the brain, such as neurons and glia, rely on the asymmetric distribution of their proteins compartmentalizing the function of dendrites, axons, glial projections and endfeet. Subcellular proteomes can be assembled either by the transport of proteins synthesized in the cell soma or by the delivery of mRNAs to target compartments where they are locally translated into protein. This latter mechanism is known as local protein synthesis or local translation, and it has been best studied in neurons. Increasing evidence suggest it is also required to maintain local protein homeostasis in glial cells, however, in microglia, local translation remains largely unexplored. Given the scant evidence, we aimed at exploring the existence of local translation in microglial peripheral processes (MPPs) and unravel its functional significance. We report that local translation indeed happens in MPPs and it is enhanced by triggering a microglial inflammatory response with bacterial lipopolysaccharides (LPS) suggesting a functional relevance of this molecular mechanism in response to inflammation. We found that *Actb* and *Par3* mRNAs polarize to MMPs and are locally translated upon LPS exposure. Interestingly, downregulation of the *Actb* binding protein IMP1/ZBP1 impaired *Actb* mRNA polarization and its localized translation, leading to defects in filopodia distribution, lamellar directed migration and phagocytosis in microglia. Thus, our work contributes to recent findings that localized translation occurs in microglia and gives a mechanistic insight into the relevance of this molecular mechanism in fundamental microglial functions in response to LPS-induced inflammation.

INTRODUCTION

Brain cells present an extremely complex and polarized morphology with cell extensions (dendrites, axons and glial peripheral processes) reaching more than a meter in length in some cases. Such complexity is required for their specific functions, and it mirrors the equally complex structure of the organ they are hosted in. Morphological and functional polarization of brain cells is achieved by asymmetrical distribution of their proteins to distinct subcellular compartments. Subcellular proteomes are assembled either by protein transport from the soma or by local translation. The latter can be accomplished by the transport of the mRNAs to the periphery followed by their translation at the target site. This mechanism enables cells to react to environmental changes in an acute manner, as proteins are produced only when and where they are needed [1].

Although local translation is a highly conserved mechanism in eukaryotic cells [2], in the nervous system it has been mostly studied in neurons where it is involved in axon guidance, arborization, and maintenance [3], synapse formation [4] and synaptic plasticity [5]. Local translation is, however, not exclusive to neurons and increasing evidence indicate that oligodendrocytes, astrocytes and radial glia also rely on this mechanism to maintain local protein homeostasis and their functional fitness [6]. Surprisingly, mRNA transport and localized translation in microglia have remained unexplored until only recently, when *Rpl4* mRNA, which encodes the 60S ribosomal protein L4, was detected in microglial processes in the mouse brain [7] and a localized ribosome-associated transcriptome was identified [8]. Additionally, in an *ex vivo* wound model,, microglial local translation was found to be relevant for efficient phagocytosis [8]. Given the scant evidence on localized translation in microglia, this proof-of-concept article aims to contribute to shed light on the relevance of local protein synthesis in regulating fundamental microglial functions in response to inflammation.

Microglia are the resident immune cells of the central nervous system, involved in brain homeostasis maintenance, and the first line of defence upon pathogen infection and brain injury. Microglia continuously survey the brain parenchyma with their peripheral processes which are continuously extending and retracting [9]. Upon pathological insults, they rapidly change their morphology by remodelling their actin cytoskeleton, leading to enlarged processes and even the acquisition of bushy and ameboid morphologies [10,11]. During neuroinflammation many secreted factors induce microglial proliferation and process migration towards the source of injury. Microglial motility depends on two peripheral F-actin-rich filamentous structures: 1) fine processes, termed filopodia, which survey the environment and respond to the inflammatory cues or chemokines by inducing intracellular signalling, and 2) large processes, termed lamellipodia, which are responsible for migration [10,12]. Interestingly, these structures where already described in axonal growth cones more than three decades ago [13]. Like in microglial peripheral processes (MPPs), growth cone filopodia sense external cues and extend towards chemoattractants or collapse in response to molecular repellents guiding lamellae towards or away from the guidance cue. Importantly, growth cone behaviour is regulated by local protein synthesis [3]. Given the similarities between axonal growth cones and MPPs we hypothesized that mRNA transport and local translation happens in microglia supporting essential functional changes in response to inflammation.

Here we show that exposure of microglia to an inflammatory challenge driven by bacterial lipopolisaccharides (LPS) induces the localization to MPPs of two key mRNAs involved in cell polarity, cytoskeletal rearrangement and migration: *Actb* and *Par3* [14,15]. One of the RNA binding proteins (RBPs) responsible for *Actb* localization is the well

characterized IGF2 mRNA binding protein 1 / zipcode binding protein 1 (IMP1/ZBP1) [16]. Importantly, *Imp1* knockout mice show defects in *Actb*-containing granule motility in dendrites and transient *Imp1* knockdown affects the dendritic distribution of *Actb* and impairs dendritic arborization. Additionally, *Imp1* haploinsufficiency decreases *Actb* mRNA localization to axons and limits the regeneration of peripheral nerves upon injury [17-19]. Interestingly, when we downregulate IMP1/ZBP1 in microglia, β-actin synthesis is decreased in MPPs resulting in impaired filopodia distribution, lamellar polarized migration and phagocytosis upon LPS exposure. Therefore, our results suggest for the first time that IMP1/ZBP1-dependent local translation is relevant for the microglial response to inflammation.

RESULTS

LPS induces local protein synthesis in microglial peripheral processes (MPPs).

To characterize RNA transport and local translation in microglia we used primary cultures and identified newly synthesized proteins by puromycin labelling. Puromycin is an aminoacyl-tRNA analogue that incorporates into nascent polypeptide chains during elongation in a ribosome-catalyzed reaction [20]. Thus, with specific anti-puromycin antibodies *de novo* protein synthesis can be detected. We exposed cultured microglia to 2 µM puromycin for 10 and 30 minutes. Nascent peptides were readily detected after a 10-minute single exposure to puromycin both in the cell soma and in MPPs (identified by phalloidin staining), and signal increased with a 30-minute puromycin pulse. To make sure that puromycilation assays are suitable to detect newly synthesized proteins in the periphery of microglia, cells were preincubated with 40 µM of the protein synthesis inhibitor anisomycin, which reduced puromycin fluorescent intensity to levels similar of that of negative controls in MPPs (Figure 1A). Furthermore, to confirm MPPs were in fact peripheral to the soma we determined the presence of the endoplasmic reticulum protein calreticulin whose expression is high in the cell bodies, while low or undetectable in peripheral processes [21]. We could not detect calreticulin signal in MPPs suggesting proteins might be synthesized locally beyond the somatic region (Figure 1B). Microglia sense signals from their environment, including inflammatory cues, with their processes [8,9]. This likely requires changes in the local proteome for cells to rapidly adapt to changes in their surroundings. Thus, we sought to address if exogenously inducing inflammation regulated the levels of newly synthesized proteins in MPPs. To that end we exposed cultured microglia to LPS, an endotoxin commonly used to induce inflammatory responses in microglia [22], and treated cells with puromycin for the last 30 mins. Puromycin fluorescence increased upon a 24-hour LPS exposure in MPPs (Figure 1C), suggesting that inflammation enhances the synthesis of proteins targeted to the periphery of microglia.

A pre-requisite for local protein synthesis is the transport of mRNAs to peripheral processes. Thus, we addressed the presence of RNA in MPPs in control and LPS-stimulated microglia using SYTO RNASelect, a fluorescent dye that selectively binds RNA [23] (Figure 2A). We analyzed SYTO-positive foci and SYTO-puromycin colocalization in microglia exposed to vehicle (PBS) or LPS for 24 hours as previously described [21]. LPS treatment increased RNA foci (SYTO puncta. Figures 2B^{i} and 2B^{ii}) in MPPs as well as SYTO-puromycin colocalization, especially at the edge of lamellipodia where fine processes (filopodia) emerge (Figures 2B^{ii} and B^{iii}). Altogether, these data suggest that LPS-induced inflammation enhances RNA levels and protein synthesis in MPPs.

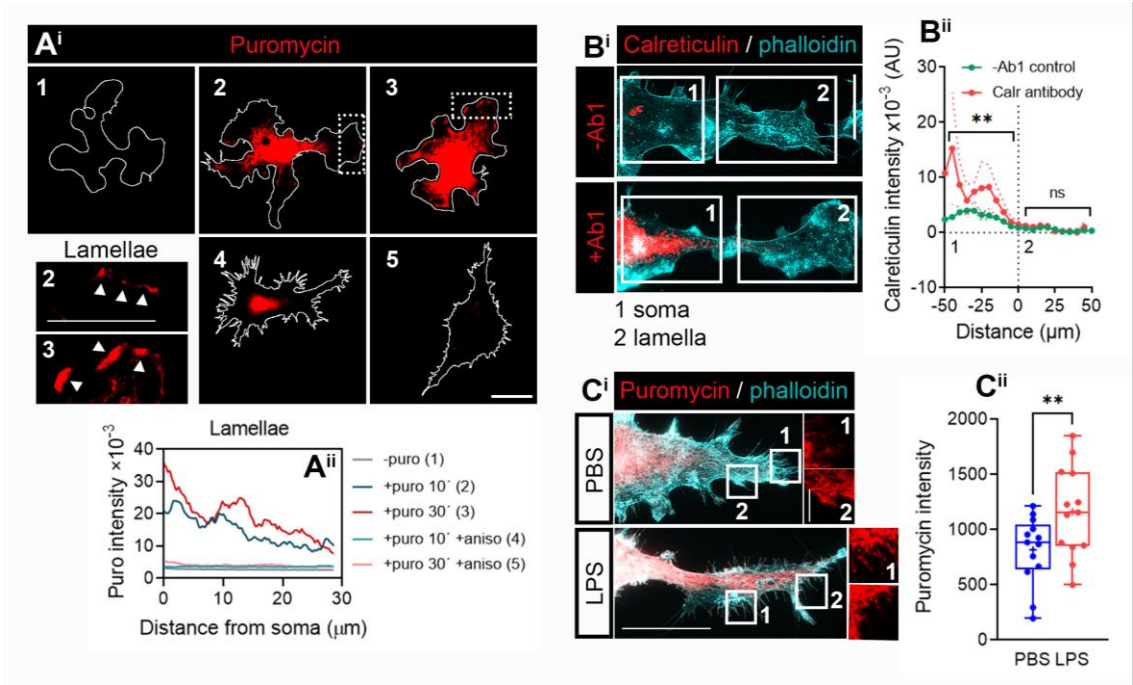

Figure 1- Newly-synthesized proteins increase in microglial peripheral structures upon LPS exposure. (A) To visualize protein synthesis in microglial peripheral structures, cells were incubated with vehicle (-puro; 1), with puromycin for 10 and 30 minutes (+ puro; 2 and 3 respectively) or with anisomycin for 30 minutes and puromycin for 10 (+ puro 10´ + aniso; 4) or 30 minutes (+ puro 30 ´ + aniso; 5). Representative micrographs of puromycin distribution in whole cells and in lamellae are shown. Scale bar, 20 µm (insets, 5µm) (A^i). The graph represents the distribution of puromycin-labelled newly synthesized proteins along lamellae (A^{ii}). **(B)** To identify the somatic domain and the peripheral structures in microglia, cells were stained with an anti-carleticulin (Carl) antibody (+Ab1) to visualize the "somatic" ER (soma, 1) and with phalloidin to visualize the actin dense lamellipodia (2). The periphery was defined as the region where Carl was undetectable compared to a no-primary antibody negative control (-Ab1) which coincides with an intense phalloidin staining. Representative micrographs of the distribution of Carl and phalloidin are shown. Scale bar, 20 µm (B^i). The graph represents the mean distribution of Carl in the soma (1) and in the periphery (2) of microglia cultured in 3 independent experiments (n=3) analyzed by two-way ANOVA followed by Holm Sidak´s multiple comparisons test **$p < 0.01$; ns, not significant. **(C)** Newly synthesized proteins were measured in the periphery of microglia treated with vehicle (PBS) or LPS for 24 hours. Puromycilated newly synthesized proteins in the periphery of phalloidin-stained microglia treated with PBS or LPS are shown. Insets (1 and 2) show puromycin labelling at the edge of lamellae where filopodia emerge. Scale bar, 20 µm (insets, 5µm) (C^i). The box and whisker graph indicates the mean fluorescence intensity of puromycin in the periphery of microglia cultured in 11 independent experiments (n=11) analyzed by two-tailed t test. **$p < 0.01$. two-tailed t test (C^{ii}).

LPS drives *Actb* and *Par3* mRNA polarization toward MPPs.

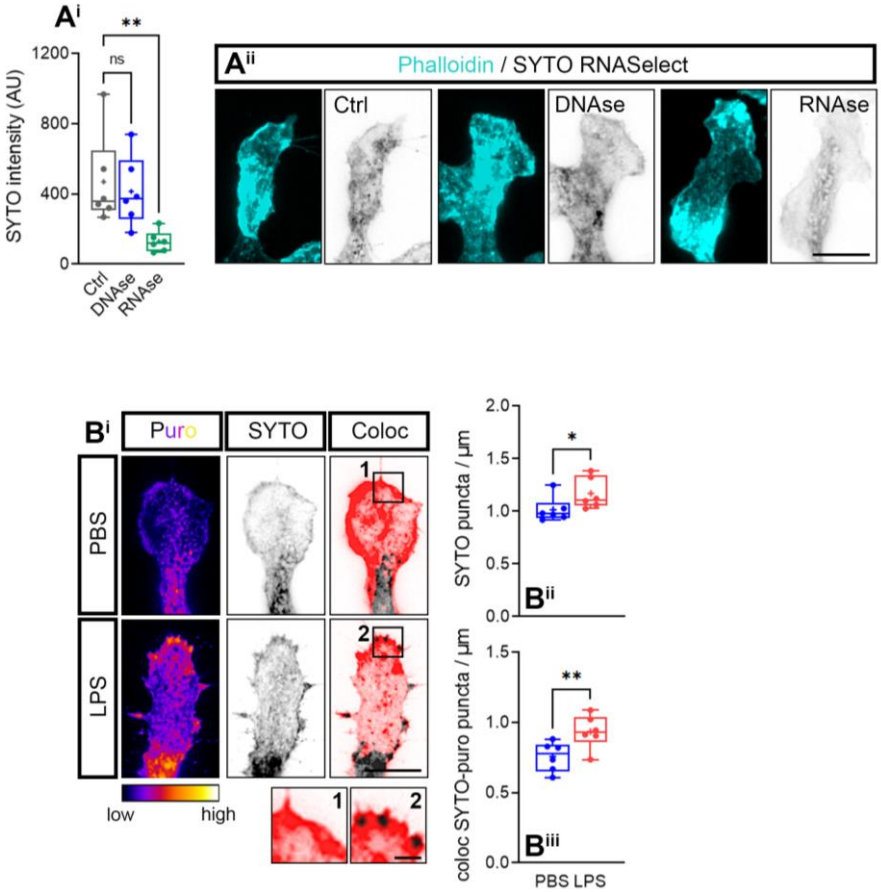

Figure 2- RNA localization and localized translation increase in microglial peripheral structures upon LPS exposure. (A) RNA localization to the periphery of microglia was visualized with SYTO RNASelect green fluorescent dye. To determine if SYTO selectively labelled RNA, fixed cells were treated with DNAse or with RNAse. The box and whisker graph indicates the mean fluorescence intensity of SYTO in phalloidin-labelled microglia from 6 independent experiments (n=6) analyzed by one-way ANOVA followed by Dunnet´s multiple comparison test. **p < 0.01; ns, not significant (A^i). Micrographs show phalloidin and SYTO labelling in control, DNAse- and RNAse-treated cells. Scale bar, 10 µm (A^{ii}). **(B)** SYTO-positive foci and puromycin-SYTO colocalization indicate increased RNA localization and localized translation in the periphery of LPS-treated microglia compared to control treatments. Puromycin (heatmaps), SYTO (greyscale) and colocalization (greyscale) in phalloidin-labelled (red) microglia is shown. Scale bar, 10 µm (insets, 2 µm) (B^i). Box and whisker graphs represent the average SYTO-positive foci (B^{ii}) and SYTO-puromycin colocalization (B^{iii}) in the periphery of PBS- and LPS-treated microglia from 6 independent experiments (n=6) analyzed by two-tailed t tests. *p < 0.05; **p < 0.01.

Like in the axonal growth cone, MPPs' fine processes (filopodia) sense external cues and extend towards chemoattractants or collapse in response to molecular repellents guiding large processes (lamellae) toward or away from the guidance cue. Importantly, growth cone behaviour is regulated by local protein synthesis. In particular, local translation of both *Actb* and *Par3* mRNAs are known to be involved in axon guidance in response to external cues [15,24]. Given the similarities between MPPs and axonal growth cones, we addressed to which extent these mRNAs localized to MPPs in response to LPS. We first analyzed the presence of *Actb* and *Par3* mRNAs in MPPs upon LPS exposure by fluorescent *in situ* hybridization (FISH). Neither *Actb* nor *Par3* could be detected above background levels (established by the FISH signal from non-targeting probes) in MPPs after a 24-hour treatment (Supplementary figures $1A^i$ and $1A^{ii}$).

However, *Actb* mRNA was readily detected in MPPs in response to a 30- minute exposure to LPS, whereas it was mainly localized to the soma in control cells (Figure 3A) and to proximal processes in mouse brains *in vivo* (Supplementary figure 2A). Indeed, frequency analysis indicated that *Actb* granules accumulated away from the nucleus in straighten cell sections in LPS-treated microglia but not in controls (Figures 3B). These results suggest that acute LPS exposure leads to the polarization of *Actb* mRNA toward MPPs. On the other hand, *Par3* mRNA was detected in MPPs in both PBS- and LPS-treated cells (Figure 3C) as well as in distal peripheral processes *in vivo* (Supplementary figure 2A), suggesting basal *Par3* localization to the periphery of microglia. However, the peripheral polarization of *Par3* granules was stronger in response to LPS exposure, as shown by frequency analyses in straighten cell sections (Figure 3D). In summary, exposure to acute LPS induces the polarization of *Actb* and *Par3* mRNAs toward MPPs.

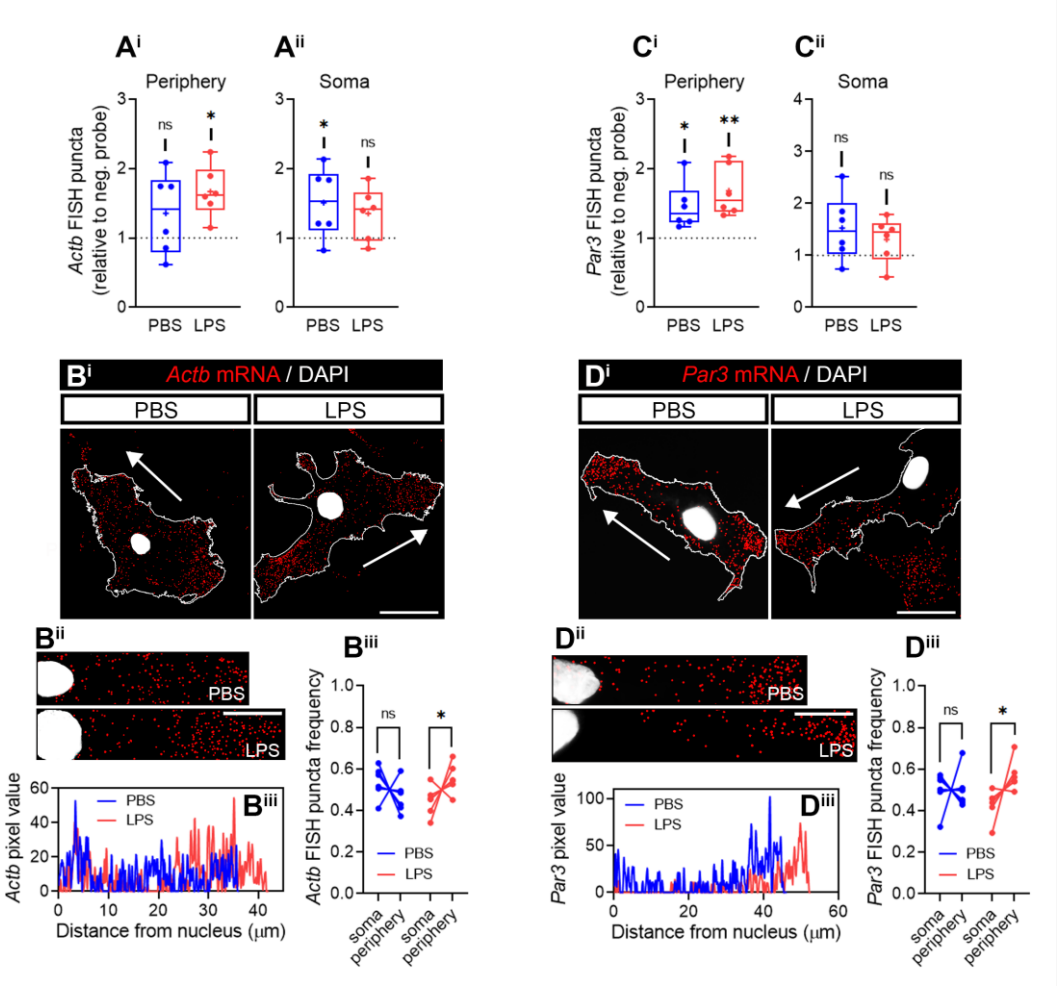

Figure 3- LPS induces polarization of mRNAs towards the periphery of microglia. (A) Box and whisker graphs represent the average *Actb*-positive foci in microglial lamellae (A^i) and in the soma (A^{ii}) of PBS- and LPS-treated microglia cultured in 6 independent experiments (n=6). One-way ANOVA followed by Dunnet´s multiple comparison test. *p < 0.05; ns, not significant. **(B)** The distribution of *Actb*-positive foci is shown. Arrows in (B^i) indicate the direction of lamellar polarization in microglia. A straighten view of lamellae shown in (B^i) is depicted in (B^{ii}) and *Actb* pixel intensity within lamellae is quantified (B^{iii}). Scale bars, 20 µm (B^i) and 10 µm (B^{ii}). The box and whisker graph represents the relative frequency distribution of *Actb* foci in the periphery and the soma of microglia after treatment with PBS or LPS for 30 minutes in 6 independent experiments (n=6). Pairwise comparisons with Holm-Šídák's correction. *p < 0.05 ; ns, not significant **(C).** Box and whisker graphs represent the average *Par3*-positive foci in microglial

lamellae (B^{i}) and in the soma (B^{ii}) of PBS- and LPS-treated microglia cultured in 6 independent experiments (n=6) analyzed by one-way ANOVA followed by Dunnet´s multiple comparison test. *p < 0.05; **p < 0.01; ns, not significant. **(D)** The distribution of *Par3*-positive foci is shown. Arrows in (B^{i}) indicate the direction of lamellar polarization in microglia. A straighten view of lamellae shown in (D^{i}) is depicted in (D^{ii}) and *Par3* pixel intensity within lamellae is quantified (D^{iii}). Scale bars, 20 µm (D^{i}) and 10 µm (D^{ii}). The box and whisker graph represents the relative frequency distribution of *Par3* foci in the periphery and the soma of microglia after treatment with PBS or LPS for 30 minutes in 6 independent experiments (n=6) analyzed by pairwise comparisons with Holm-Šídák's correction. *p < 0.05 ; ns, not significant.

LPS induces *Actb* and *Par3* localized translation in MPPs.

To address if *Actb* and *Par3* mRNA polarization upon acute LPS exposure was accompanied by changes in local translation we performed proximity ligation assays (PLA) combining specific antibodies against puromycin and the protein of interest (either β-actin or Par3). This technique enables the detection of newly synthesized target proteins during the timeframe of puromycin labelling [25]. Since levels of newly produced proteins are typically lower in the processes than their soma-produced counterparts [21], to ensure the PLA signal was protein synthesis-specific we exposed cultured microglia to PBS or LPS for 30 minutes and co-incubated the cells with vehicle or with 40 µM of the protein synthesis inhibitor anisomycin. Nascent polypeptides were labelled with puromycin for the last 10 minutes of treatment. Levels of newly synthesized β-actin (Figures $4A^{i}$ and $4A^{ii}$) and Par3 (Figures $4B^{i}$ and $4B^{ii}$) were blocked by anisomycin in LPS- but not in PBS-treated cells. Similar results were obtained for Par3 when cells were exposed to LPS for 24 hours (Supplementary figure 2B). Hence, we concluded that localized translation of both mRNAs of interest occurs in MPPs at least in cells acutely treated with LPS.

Actb mRNA is the prototypical example of a localized transcript in many eukaryotic cells and its local translation is involved in cytoskeletal rearrangements, cell polarity and lamellar migration towards attractant cues [26]. Thus, we further focused on β-actin synthesis in MPPs. To confirm that β-actin-puromycin PLA signal in microglial processes was indeed local, we performed a 2-minute puromycin pulse in PBS- and LPS-treated cells. Acute treatment with LPS increased newly synthesized β-actin in MPPs compared to PBS treatment and this effect was blocked in the presence of anisomycin (Figure $4C^{i}$ and $4C^{ii}$). These data strengthen the idea that *Actb* mRNA is transported to and translated in MPPs in response to acute LPS treatment.

RNA binding protein IMP1/ZBP1 drives *Actb* mRNA localization and localized translation in MPPs.

Zipcode binding protein 1 (IMP1/ZBP1) was the first RNA-binding protein (RBP) associated to the localization of *Actb* to fibroblast lamellipodia [16]. Since then, IMP1-dependent asymmetric distribution of *Actb* has been described in many cell types, including neurons . Given the role of IMP1/ZBP1 in *Actb* mRNA localization we aimed to explore if it played a similar role in microglia.

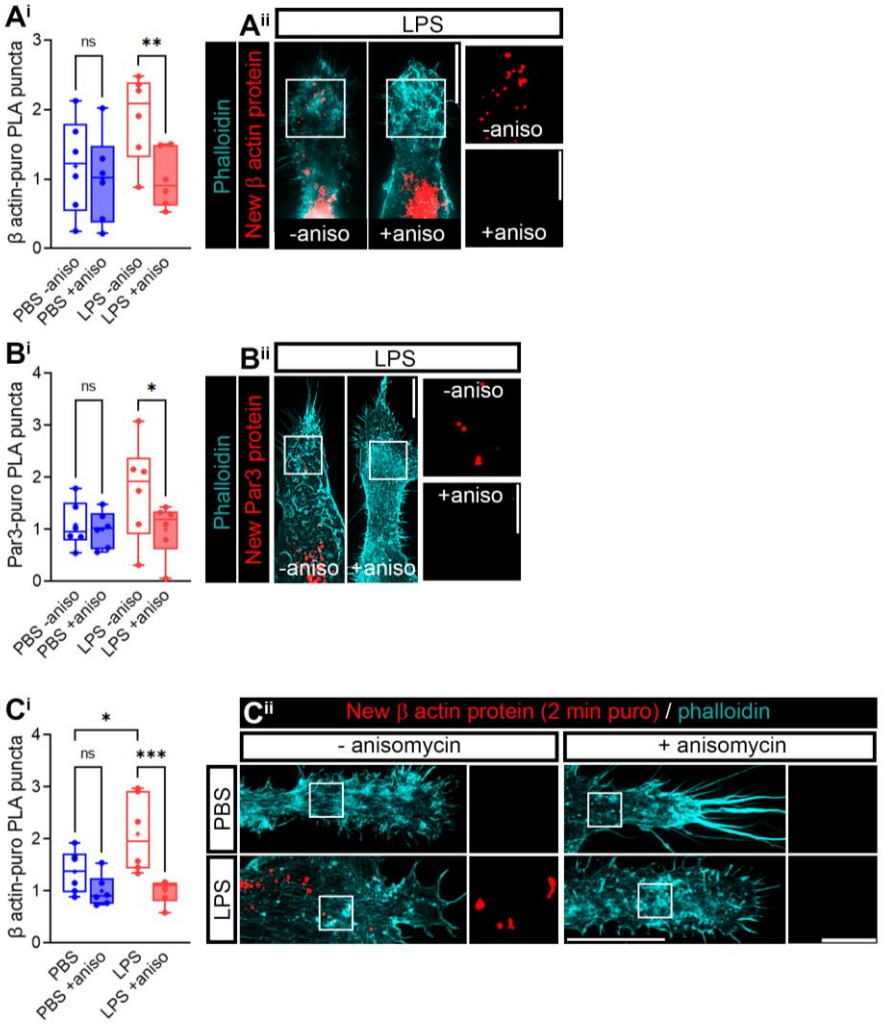

Figure 4- LPS enhances localized translation in the periphery of microglia. (A) New synthesis of β actin in microglial peripheral structures was assessed with a 10-minute puromycin pulse in PBS- and LPS-treated cells followed by proximity ligation assay (PLA) with antibodies against puromycin and β actin. As a negative control, cells were preincubated with the protein synthesis inhibitor anisomycin. The box and whisker graph represents the average PLA puncta within lamellae in phalloidin-stained microglia treated with PBS or LPS analyzed by pairwise comparisons with Holm-Šídák's correction. *p < 0.05; ns, not significant (A^i). Representative micrographs of PLA puncta in LPS-treated cells are shown. Scale bar, 10 µm (insets, 5 µm) (A^{ii}). **(B)** New synthesis of Par3 in microglial peripheral structures was assessed with a 10-minute puromycin pulse in PBS- and LPS-treated cells followed by PLA with antibodies against puromycin and Par3. As a negative control, cells were preincubated with the protein synthesis inhibitor anisomycin. The box and whisker graph represents the average of PLA puncta within lamellae in phalloidin-stained microglia treated with PBS or LPS analyzed by pairwise comparisons with Holm-Šídák's correction. *p < 0.05; ns, not significant (B^i). Representative micrographs of PLA puncta in LPS-treated cells are shown. Scale bar, 10 µm (insets, 5 µm) (B^{ii}). **(C)** Local β actin synthesis was assessed with a 2-minute puromycin pulse in PBS- and LPS-treated cells followed by PLA with antibodies against puromycin and β actin. As a negative control, cells were preincubated with the protein synthesis inhibitor anisomycin. The box and whisker graph represents the average of PLA puncta within lamellae in phalloidin-stained microglia treated with PBS or LPS. One-way ANOVA followed by Holm-Šídák's multiple comparison test. *p < 0.05; ***p<0.001; ns, not significant (C^i). Representative micrographs of PLA puncta in PBS- and LPS-treated cells are shown. Scale bar, 10 µm (insets, 2 µm) (C^{ii}).

First, we analyzed the expression of IMP1/ZBP1 in microglia and observed a granular pattern. A nonsignificant trend toward a decrease was found upon LPS exposure. (Figure 5A^{i}). However, IMP1/ZBP1-positive foci were restricted to the somatic region in control cells whereas upon LPS treatment they distributed more peripherally (Figure 5A), partially mirroring the change in *Actb* distribution upon LPS exposure. Since limiting the amount of IMP1/ZBP1 is sufficient to decrease *Actb* mRNA availability in axons [18], we sought to downregulate this RBP by genetic silencing in microglia. We transfected cultured microglia with two nonoverlapping siRNAs against *Imp1* (siRNA #1 and siRNA #2) and used a non-targeting siRNA as a negative control. Whereas siRNA #1-transfected cells showed a trend towards a decrease in IMP1/XBP1 levels after 24-hour transfection, siRNA #2 significantly downregulated the target protein both at 6 and 24 hours (Supplementary figure 2B^{i} and 2B^{ii}). Thus, we further used siRNA #2, hereafter *Imp1* KD. As shown before, *Actb* mRNA foci were significantly increased in MPPs in response to LPS in control-transfected cells (ctrl KD), in line with results obtained from untransfected cells (Figure 3A and B). Interestingly, the effect of LPS was blocked by *Imp1* KD (Figure 5B^{i} and 5B^{ii}). Furthermore, *Actb* mRNA foci frequency was lower in the soma of LPS- compared to PBS-treated and higher in the periphery (Figure 5B^{iii}) in ctrl KD cells. However, *Imp1* KD led to a loss of *Actb* polarization toward MPPs in LPS-treated cells (Figure 5B^{iii} and B^{iv}).

Next, we sought to determine in *Imp1* KD also affected local β-actin synthesis in MPPs. We performed PLA assays to detect newly synthesized β-actin following a 2- minute puromycin pulse. Like in untransfected cells (Figure 4C), acute LPS exposure in control-transfected cells led to an increase in local *Actb* translation, which was blocked by preincubation with 40 µM anisomycin. *Imp1* KD overall decreased β-actin PLA signal levels and no detectable protein synthesis was observed neither in PBS- nor LPS-treated cells above levels observed in the presence of anisomycin (Figure 5C^{i} and C^{ii}).

Altogether these results indicate that IMP1/ZBP1 regulates *Actb* mRNA localization to MPPs and its localized translation in response to LPS.

IMP1/ZBP1 downregulation impairs filopodia distribution, lamellar polarized migration and phagocytosis in microglia.

IMP1/ZBP1 knockdown alters *Actb* mRNA transport and its localized translation in MPPs. Since locally synthesized β-actin is critical for cell polarity and directional movement in eukaryotic cells [14], our next step was to address any morphological changes in peripheral processes occurring in response to acute LPS treatment and when local β-actin availability was limited in MPPs. Although LPS did not alter the number of filopodia or the morphology of lamellipodia (Supplementary figures 3A and 3B), it did modify filopodia distribution along the lamellar surface. We observed that most of fine processes were distributed to the tip and the base of lamellae in PBS-treated microglia and redistributed more homogenously upon LPS exposure when cells were transfected with a control siRNA for 24 hours. However, filopodia distribution was similar of that of control microglia in *Imp1*-transfected cells even when exposed to LPS. These results suggest that LPS leads to the rapid rearrangement of filopodia in an IMP1/ZBP1-dependent manner.

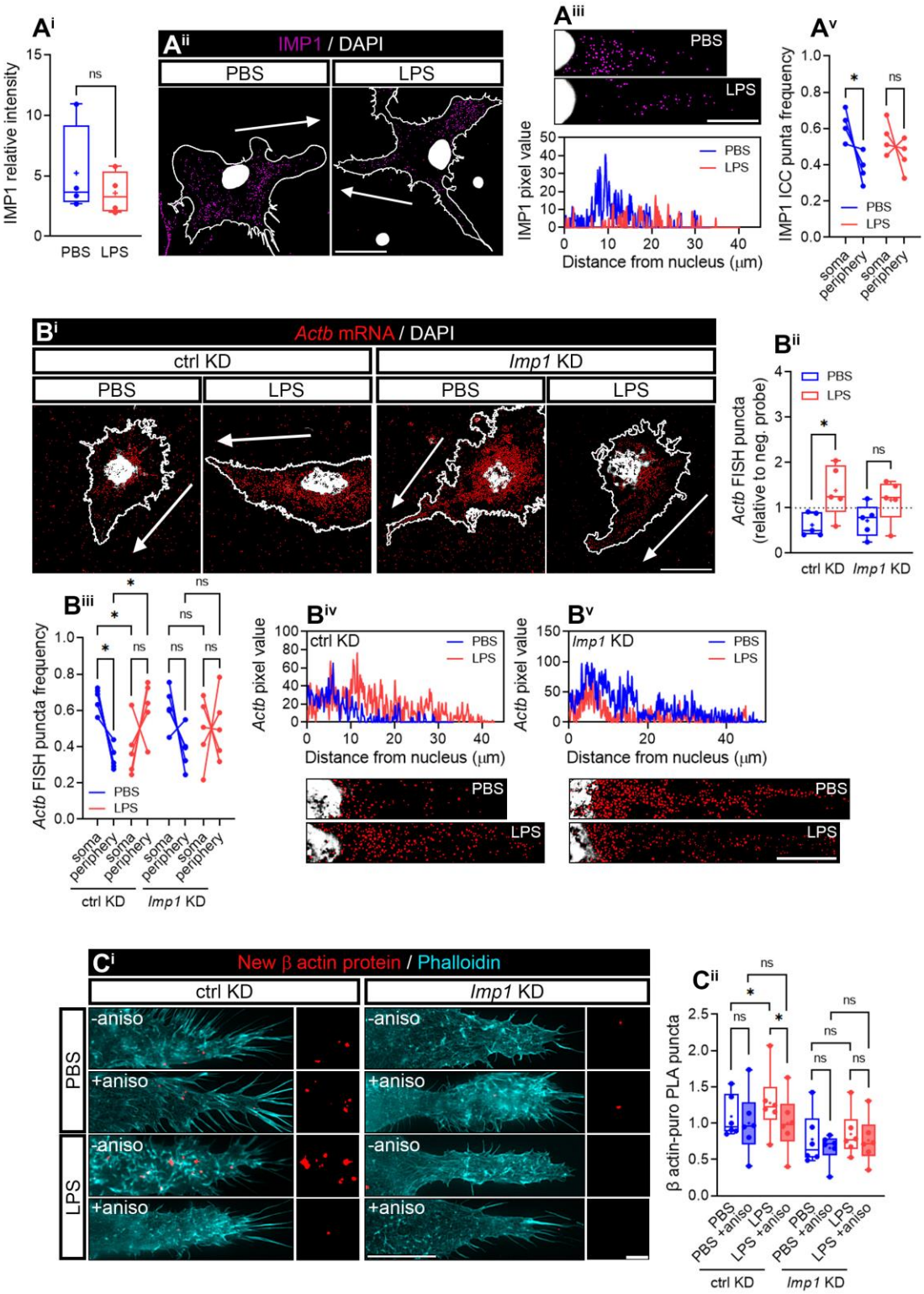

Figure 5- RNA binding protein IMP1/ZBP1 is differentially localized in PBS- and LPS-treated cells and regulates mRNA localization and localized translation in microglia. (A) Relative levels and distribution of IMP1 in PBS- and LPS-treated microglia. The box and whisker graph represents the relative IMP1 levels in microglia exposed to PBS or LPS for 30 minutes in 4 independent experiments (n=4). Two-tailed t test. ns, not significant (A^{i}). The distribution of IMP1-positive foci is shown. Arrows indicate the direction of lamellar polarization in microglia (A^{ii}). A straighten view of lamellae shown in (A^{ii}) is depicted in (A^{iii}) and IMP1 pixel

intensity within lamellae is quantified (A^{iv}). Scale bars, 20 µm (A^{ii}) and 10 µm (A^{iii}). The box and whisker graph represents the relative frequency distribution of IMP1 foci in the periphery and the soma of microglia after treatment with PBS or LPS for 30 minutes in 4 independent experiments (n=4) analyzed by pairwise comparisons with Holm-Šídák's correction. *$p < 0.05$; ns, not significant. **(B)** *Imp1* knockdown (KD) alters *Actb* mRNA localization towards the periphery of microglia. The distribution of *Actb*-positive foci is shown. Arrows in (B^{i}) indicate the direction of lamellar polarization. Scale bar, 20 µm. The box and whisker graph represents the average *Actb*-positive puncta within lamellae in microglia treated with PBS or LPS and transfected with a control (ctrl KD) or an *Imp1*-targeting *(Imp1* KD) siRNA in 5 independent experiments (n=5). One-way ANOVA followed by Holm-Šídák's multiple comparison test. *$p < 0.05$; ns, not significant (B^{ii}). The relative frequency distribution of *Actb* foci in the periphery and the soma of microglia transfected with a control (ctrl KD) siRNA or an *Imp1* siRNA (*Imp1* KD) and exposed to PBS or LPS for 30 minutes in 6 independent experiments (n=6) is plotted in (B^{iii}). Two-way ANOVA followed by Holm-Šídák's multiple comparison test. *$p < 0.05$; ns, not significant. Examples of *Actb* pixel intensity within lamellae of control- (B^{iv}, ctrl KD) and *Imp1* siRNA-transfected cells (B^{v}; *Imp1* KD) are shown. Scale bar, 10 µm. **(C)** *Imp1* KD blocks LPS-induced localized translation in microglia. Local β actin synthesis was assessed with a 2-minute puromycin pulse in PBS- and LPS-treated cells and transfected with control (ctrl KD) or *Imp1* siRNAs (*Imp1* KD), followed by PLA with antibodies against puromycin and β actin. As a negative control, cells were preincubated with the protein synthesis inhibitor anisomycin. Representative images of microglial PLA-labelled lamellae and stained with phalloidin are shown. Scale bar, 10 µm (insets, 5µm) (C^{i}). The box and whisker graph represents the average of PLA puncta within lamellae in phalloidin-stained microglia cultured in 6 independent experiments (n=6) anayzed by two-way ANOVA followed by Holm-Šídák's multiple comparison test. *$p < 0.05$; ns, not significant (C^{ii}).

We further addressed the impact of LPS and IMP1/ZBP1 on microglial migration, which depends on process motility, using a transwell system that creates two separate compartments in culture. Cells were seeded on top of a 3 µm-pore membrane (upper compartment) which enabled microglial migration toward the lower compartment (Figure 6B; Supplementary figure 3C). Acute LPS treatment had no effect on cell migration in untransfected cells (Supplementary figure 3C^{i} and 3C^{iii}) or in control- and *Imp1*-transfected cells (Figure 6B^{ii}). Similarly, the area covered by F-actin did not change in any of the experimental conditions analyzed (Figure 6B^{ii}; Supplementary figure 3C^{ii}). Then we tested process migration using 1µm-pore transwells, that restricted cell body migration (Supplementary figure 3D). In this culture setup we found that LPS did enhance MPP polarized migration as measured by the area covered by F-actin (Supplementary figure 3D^{i} and 3D^{ii}) and the effect of LPS was significantly reduced upon IMP1/ZBP1 downregulation (Figure 6C). Thus, limiting the amount of IMP1/ZBP1 and consequently local β-actin synthesis decreases LPS-dependent MPP migration.

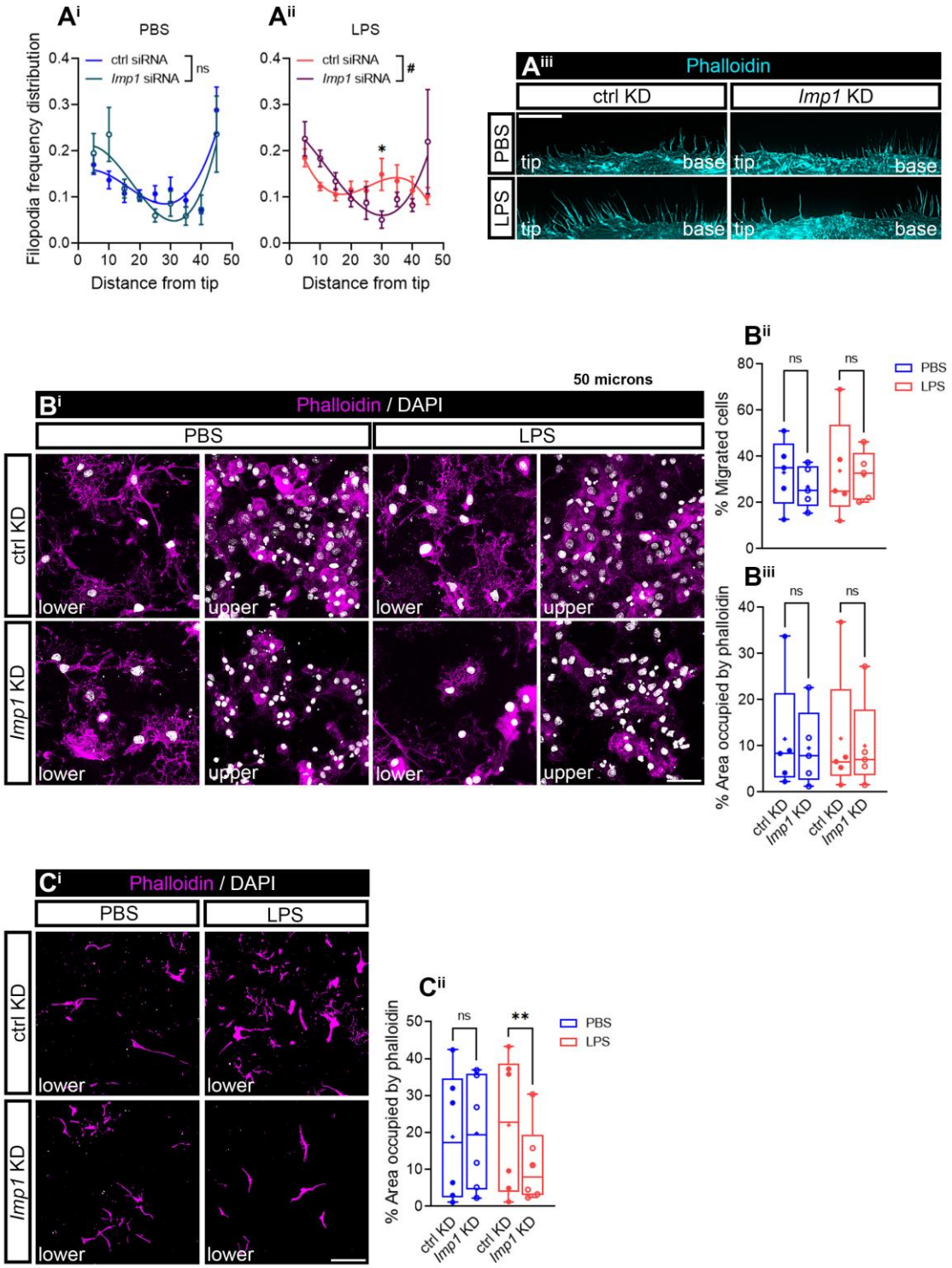

Figure 6- IMP1/ZBP1 downregulation alters the relative distribution of filopodia along microglial lamellae and blocks LPS-induced lamellar polarized migration. (A) Distribution of filopodia along microglial lamellae in control- (ctrl KD; A^{i}) and *Imp1* siRNA-transfected cells (*Imp1* KD; A^{ii}) exposed to PBS or LPS for 30 mins. Graphs represent the relative filopodia distributions of microglia cultured in 6 independent experiments (n=6). Two-way ANOVA followed by Holm-Šídák's multiple comparison test. #$p < 0.05$ (factor interaction); *$p < 0.05$; ns, not significant.. Representative micrographs depicting filopodia distribution in phalloidin-stained microglia are shown. Scale bar, 10 µm (A^{iii}). **(B)** To address microglial migration, cells were

cultured in 3-µm-diameter transwell membranes. PBS or LPS were applied to the bottom of the transwell for 30 minutes. Representative images of cells migrated to the lower side of the membrane and those remaining in the upper compartment are shown. Scale bar, 50 µm (B^{i}). The percentage of cells migrated to the lower side of the membrane (B^{ii}), as well as the relative coverage of phalloidin staining (B^{iii}) were calculated in 5 independent experiments (n=5) and are represented in the box and whisker graphs. One-way ANOVA followed by Holm-Šídák's multiple comparison test. ns, not significant. **(C)** To address lamellar migration we restricted the soma to the upper compartment by culturing cells in 1-µm-diameter transwell membranes. PBS or LPS were applied to the bottom to the lower compartment for 30 minutes. Representative images of lamellae migrated to the lower side of the membrane are shown. Scale bar, 50 µm (C^{i}). The box and whisker graph represents the relative coverage of phalloidin staining at the lower side of the membrane. Analyses were performed in 6 independent experiments (n=6) by one-way ANOVA followed by Holm-Šídák's multiple comparison test. $^{**}p < 0.01$; ns, not significant; test (C^{ii}).

Finally, we tested the effect of IMP1/ZBP1 on phagocytosis of apoptotic cells, which is one of the main functions of microglia to restore brain homeostasis by removing cell debris and damaged cells upon inflammation, and it is driven by MPPs *in vivo*. During phagocytosis, MPPs rearrange their cytoskeleton and form specialized peripheral structures termed phagocytic pouches [22]. Interestingly, Vasek and colleagues have recently reported a localized translatome in microglia enriched in phagocytic pouches, and that local protein synthesis is required for efficient microglial phagocytosis [8]. Given that local β-actin production is required for rapid cytoskeletal remodelling in response to external guidance cues [24], and that our own data indicate that *Imp1* KD impairs *Actb* translation in MPPs (Figure 5C), filopodia distribution (Figure 6A) and LPS-dependent polarized MPP migration (figure 6C), we sought to analyze the relevance of IMP1/ZBP1 on phagocytosis.

We treated cells with PBS or LPS for 30 minutes prior to adding apoptotic cells. We fed cultured microglia with human SH-SY5Y vampire red transgenic apoptotic neurons for 1 hour and analyzed the percentage of microglia with vampire-positive particles inside. Around 60% of microglia had engulfed apoptotic neurons both in control and LPS-induced conditions (Supplementary figure $3E^{i}$). However, engulfed particles were smaller in LPS-treated cells compared to controls (Supplementary figures $3E^{ii}$ and $3E^{iii}$). These results suggest that LPS has an effect in apoptotic cell degradation. We then performed experiments in microglia transfected with control or *Imp1* siRNAs for 24 hours. We reproduced the effect of LPS on particle size in control-transfected cells (Supplementary figure $3E^{iv}$). Interestingly, *Imp1* KD did not change the percentage of phagocytic microglia but it increased vampire particle size in LPS-treated cells (Figures 7A). Additionally, IMP1/ZBP1 downregulation led to a higher proportion of LPS-treated microglia with a smaller number of vampire particles (1-5) and a decrease in cells with higher number of phagocytosed neurons (6-10; Figure 7B). Altogether, these results indicate that IMP1/ZBP1 is required for efficient LPS-induced phagocytosis.

In summary, our data confirm that microglia are able to produce proteins locally at their MPPs [8]. In addition, we identified *Actb* as one of the transcripts whose localized translation is induced by the inflammatory cue LPS. As in other polarized cells, *Actb* localization and localized translation in microglial MPPs is regulated by the RBP IMP1/ZBP1, and our results suggest that IMP1/ZBP1-dependent β-actin local synthesis is involved in fundamental microglial functions, including filopodia rearrangements, polarized migration and phagocytosis.

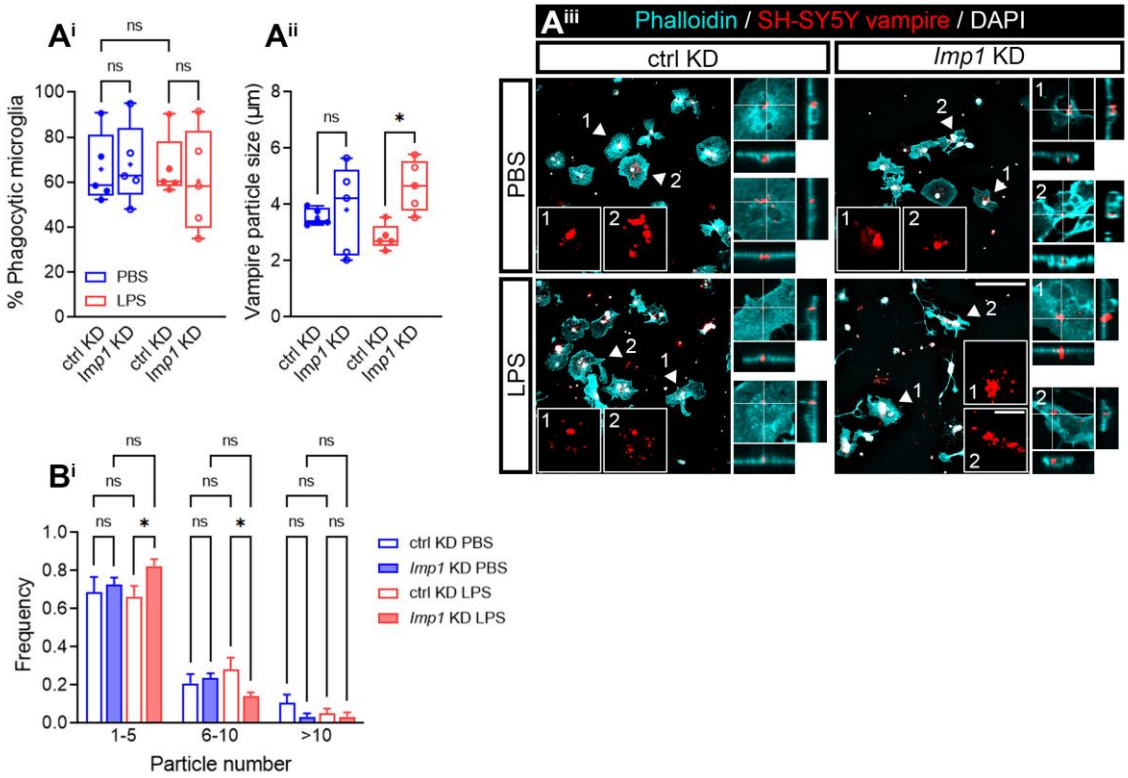

Figure 7- IMP1/ZBP1 downregulation impairs microglial phagocytosis. (A) Percentage of control- (ctrl KD) and *Imp1*-transfected (*Imp1* KD) phagocytic microglia after treatment with SH-SY5Y apoptotic neurons labelled with vampire for 1 hour after by exposure to PBS or LPS for 30 minutes (A^i). Vampire particle size in phagocytic microglia following the same experimental setup as in (A^i) (A^{ii}). Both graphs correspond to 5 independent experiments (n=5). Two-way ANOVA followed by Holm-Šídák's multiple comparison test was performed. *$p < 0.05$; ns, not significant. Representative micrographs of vampire-positive neurons (red) inside phalloidin-stained microglia are shown. Insets depict examples of vampire particles inside phagocytic microglia. Zoomed orthogonal views are also represented for each experimental condition. Scale bar, 100 µm; 10 µm in insets and orthogonal view (A^{iii}). **(B)** Frequency distribution of phagocytic microglia with 1-5, 6-10 and >10 apoptotic neurons inside, following transfection with control (ctrl KD) and *Imp1* (*Imp1* KD) siRNAs and treated with PBS or LPS for 30 minutes. The graph represents the mean + SEM of 5 independent experiments (n=5). Two-way ANOVA followed by Holm Sidak´s multiple comparison test was performed, *$p < 0.05$; n.s, not significant. Only the following comparisons are plotted for simplification purposes: PBS vs LPS in control-transfected cells, PBS vs LPS in *Imp1*-transfected cells, control- vs *Imp1*-transfected cells and exposed to PBS, control- vs *Imp1*-transfected cells and exposed to LPS.

DISCUSSION

Here we report that LPS triggers within minutes the translation in MPPs of two transcripts involved in cell polarization, cytoskeletal rearrangement and migration, one of them being *Actb*. Downregulation of the RBP IMP1/ZBP1 impairs *Actb* localized translation and leads to defects in LPS-dependent filopodia rearrangements, MPP migration and phagocytosis. Thus, the microglial response to acute inflammation functionally requires local protein synthesis within MPPs.

This work was motivated by evidence that microglia, like many other highly polarized cells, sense local changes in their environment with their peripheral processes which respond independently from their cell soma. Local MPP responses, including process migration or phagocytosis are required to maintain brain homeostasis, which might be imbalanced by pathological insults like neuroinflammation [12,22]. Thus, microglia rely on efficient signalling initiated at MPPs [12], which we reasoned could be accompanied by changes in the local proteome. Local proteomes can be shaped by proteins transported from the soma or by those synthesized locally in MPPs. Indeed, in neurons, oligodendrocytes, astrocytes and radial glia, local protein synthesis is required to maintain local protein homeostasis and for cells to accurately respond to environmental cues, as proteins are produced only when and where they are needed [1,6]. In the case of microglia however, local translation had not been described until recently [8]. Given the limited information from microglial cells, we sought to explore this molecular mechanism based on the similarities between axonal growth cones and MPPs.

MPPs highly resemble axonal growth cones in terms of their morphology and behaviour. Both contain fine processes, termed filopodia, which survey their environment. Upon environmental changes that induce migratory responses, filopodia extend or collapse and drive large processes (lamellipodia) towards chemoattractants or away from chemorepellents. During development growth cones respond to NGF and netrin-1 by locally translating *Par3*, which leads to axonal outgrowth [15]. Similarly, β-actin is locally produced in response to netrin-1 and enables actin cytoskeleton polymerization and reorganization leading to axon elongation [24]. Hence, we asked if *Actb* and *Par3* mRNAs where also locally translated in MPPs and to what extent were mRNA localization and localized translation required for the functional response of microglia to inflammation. Our results indeed confirmed that both transcripts polarized toward MPPs and were locally translated upon inducing an acute inflammatory state in microglia. Interestingly, neither *Actb* nor *Par3* could be detected in MPPs when challenging microglia with LPS for 24 hours, although we could not rule out *Par3* translation at this time point. These results suggest that translation of a distinct cohort of localized mRNAs might be required for microglia to differentially adapt to acute and chronic insults. This is reminiscent of the axonal response to pathological stimuli. For instance, long exposure of axons to Aβ oligomers, involved in Alzheimer´s disease, drives the local translation of the transcription factor *Atf4*, which is not triggered by acute Aβ treatment. Importantly, late axonal synthesis of ATF4 itself depends on an early local production of vimentin [27]. Thus, distinct waves of local translation are required for cells to adapt to the nature and duration of stimuli, and local transcriptomes and translatomes likely need to be dynamically regulated in time to continuously support the accurate response of peripheral processes, including MPPs, to environmental changes.

For local translation to occur, mRNAs and components of the protein synthesis machinery must be transported to the target peripheral compartment. Following transcription, RBPs bind mRNAs through the recognition of cis-localization elements

typically present in the 3' untranslated region (3'UTR) of the transcripts [28]. The resulting ribonucleoprotein complexes (RNPs) are transported by molecular motors in a translationally repressed state. Once localized to their destination and upon stimulation mRNAs are released from the RNPs, associate to the localized protein synthesis machinery and translate into proteins [3]. In order to address the functional relevance of local translation in microglia, we downregulated IMP1/ZBP1, which was the first RPB associated to the localization of *Actb* to fibroblast lamellipodia [16]. Since then, IMP1-dependent asymmetric distribution of *Actb* and its involvement in local translation have been described in many cell types, including neurons. Importantly, *Imp1* haploinsufficiency decreases *Actb* mRNA localization to axons and limits the regeneration of peripheral nerves upon injury [18]. Thus, we reasoned that limiting the availability of IMP1/ZBP1 in microglia would affect LPS-dependent β-actin synthesis in MPPs and it could uncover a functional relevance of local translation in the microglial response to inflammation. Indeed, genetic silencing experiments did confirm that IMP1/ZBP1 is required for *Actb* mRNA polarization to and localized translation within MPPs in response to LPS. More importantly, acute LPS exposure seemed to induce changes only in the behaviour of MPPs. For instance, LPS drove filopodia rearrangements along lamellipodia but did not affect lamellar morphology. On the other hand, whole cell migration was not affected by LPS treatment, which conversely induced MPP directed motility when restricting somatic migration. It is precisely in both these contexts that IMP1/ZBP1-dependent local β-actin synthesis seemed to play a relevant role, evidencing the dependency of microglia on local translation to rapidly react to environmental changes sensed by their peripheral processes. One very relevant function carried out by microglia is phagocytosis, which is essential to restore brain homeostasis by removing cell debris and damaged cells upon inflammation. Phagocytosis is performed by MPPs *in vivo* and requires rapid morphological changes of processes to form the so called phagocytic pouches, independently from the cell soma [22]. Importantly, ribosome-bound transcripts involved in phagocytosis are enriched in MPPs *in vivo* and *de novo* protein synthesis is required for the formation of phagocytic pouches *ex vivo* [8]. In line with these observations our results showed IMP1/ZBP1 downregulation impaired LPS-dependent phagocytosis of apoptotic neurons, confirming the functional relevance of RBP-mediated local protein synthesis in response to inflammation.

In recent years, dysregulated RNA localization and localized translation in neurons have been associated to neurological diseases pointing towards the importance of these molecular mechanisms in supporting axonal, dendritic and synaptic functions, as reviewed [6]. Importantly, many genetic neurological disorders, such as fragile X syndrome (FXS), amyotrophic lateral sclerosis (ALS), spinal muscular atrophy (SMA) or Hungtinton´s disease are characterized by mutations in RBPs, and defects in RNA localization and/or local translation are common to all of them. IMP1/ZBP1 has been reported to bind several mRNAs encoded by autism spectrum disorder-genes [29] and our findings indicate that limiting IMP1/ZBP1 availability disrupts mRNA localization and translation in MPPs, and leads to dysfunctional microglia. Thus, it is tempting to speculate that defects in RBPs not only impair local protein synthesis in neurons, but also in microglia contributing to neurological disorders.

One of the limitations of this study is that mechanistic experiments have been performed *in vitro* using siRNAs as the only genetic tools for local translation inhibition, one of the reasons being the difficulty to genetically-manipulate microglia by transfection and transduction both *in vitro* and *in vivo* [30]. Now that microglia are finally in the arena of the local translation field, it will be interesting to develop novel tools to

address to what extent defects in RBPs and dysregulated local protein synthesis lead to microglia dysfunction and contribute to the development of brain pathologies in disease models. However, our proof-of-concept work already provides an unprecedented mechanistic insight into local translation regulation in microglia and points towards deficient response to inflammation when local β-actin synthesis in MPPs is impaired.

MATERIALS AND METHODS

Animals.

All animal protocols followed the European directive 2010/63/EU and were approved by the UPV/EHU ethics committee. For microglial cultures, Sprague-Dawley rats were bred in local facilities and embryonic brains were obtained from CO_2 euthanized pregnant rats. Mice (3-month-old male and female) were euthanized by anaesthesia followed by transcardiac perfusion with saline solution.

Primary microglia cultures.

Cortical microglial cells were isolated from mixed glial cultures. Briefly, brain hemispheres were dissected from postnatal Sprague Dawley rats (P0-P2) and dissociated with 0.25% trypsin (Sigma Aldrich, Merck, Darmstadt, Germany) and 0.004% DNAse (Sigma Aldrich) for 15 minutes at 37ºC. Trypsinization was stopped by adding glial plating medium containing IMDM (Gibco, Thermo Fisher Scientific, Waltham MA, USA), 10% fetal bovine serum Hyclone (Cytiva, Thermo Fisher Scientific) and 10% of a mixture of antibiotics and antimycotics (Gibco). Cells were homogenized and centrifuged at room temperature for 6 minutes at 1200 rpm, resuspended in 1 ml plating medium and mechanically dissociated using 21G and 23G needles. Cells were centrifuged at room temperature for 6 minutes at 1200 rpm, resuspended in plating medium and seeded onto 75 cm^2 flasks (BioLite, Thermo Fisher Scientific). Cultures were maintained at 37 ºC in a 5% CO^2 humidified incubator. After 1 day in vitro (DIV) the medium was replaced with glucose Dulbecco's Modified Eagle's Medium (DMEM, Gibco) containing 10% fetal bovine serum (Sigma Aldrich), 1 U/ml penicillin, 1 µg/ml streptomycin and 292 µg/ml glutamine (all from Gibco). The medium was replaced every 3 days.

For microglia isolation, 10-17 DIV mixed glial culture flasks were agitated at 180 rpm for 4h at 37 ºC. The medium was collected and centrifuged at room temperature for 6 minutes at 1200 rpm. Cells were resuspended in serum-free medium containing Neurobasal, 1X B-27 supplement and 2 mM L-glutamine (all from Gibco). Microglia were seeded on Poly-D-lysine(PDL)-coated coverslips (40.000-80.000 cells/cm^2) or on 1- and 3-µm pore transwells (60.000-80.000 cells/cm^2). Treatments were performed at 12-14 DIV or 19-21DIV.

Pharmacological treatments.

Lipopolysaccharides from *Escherichia coli* (BioXtra, Sigma Aldrich) were added to cells at 150 ng/ml for 30 minutes or 24 hours. PBS was used as vehicle control.

For puromycilation assays cells were exposed to 2 µM puromycin dihydrochloride from *Streptomyces alboniger* for 2, 10 or 30 minutes (Sigma Aldrich). Water was used as a vehicle control. Whenever stated, cells were preincubated for 30 minutes with anisomycin (Sigma Aldrich) at 40 µM to block protein synthesis.

Immunocytochemistry.

Microglia were fixed for 20 min at 4 ºC in 4% PFA, 4% sucrose in PBS. Cells were washed three times for 5 minutes with PBS, permeabilized and blocked for 30min in 3 % BSA, 100 mM glycine and 0.25% Triton X-100 (all from Thermo Fisher Scientific). Cells were incubated overnight at 4 ºC with primary antibodies against puromycin (mouse monoclonal 1:500, Merck), Par3 (rabbit polyclonal 1:1000, Sigma Aldrich), β-actin (rabbit polyclonal 1:200, Sigma Aldrich), IMP1/ZBP1 (mouse monoclonal 1:500, MBL, Woburn MA, USA or rabbit monoclonal 1:50, Abcam, Cambridge, UK), calreticulin (rabbit polyclonal 1:500, Abcam, Cambridge, UK) and Iba1 (guinea pig, polyclonal 1:500, Synaptic Systems, Göttingen, Germany). Samples were washed three times for five minutes with PBS and incubated with the corresponding fluorescently labelled secondary antibodies for 1 hour at room temperature (all from Invitrogen, Thermo Fisher Scientific). Cells were washed three times with PBS and, whenever stated, labelled with Alexa Fluor 488-conjugated phalloidin (1:800, Thermo Fisher Scientific) in PBS or Alexa Fluor 647-conjugated phalloidin (1:1000, Abcam) in 1% BSA for 30 minutes at room temperature. Samples were washed three times with PBS and mounted with Prolong Gold Antifade mounting medium with DAPI (Invitrogen, Thermo Fisher Scientific).

SYTO RNA Select labelling.

Cultured cells were washed once with cold PBS, once with 50% methanol in PBS and fixed in cold 100% methanol for 5 minutes. Samples were rehydrated by washing them in 50% methanol in PBS once and in PBS three times at room temperature. Cells were incubated for 20 min at room temperature with 500 nM SYTO RNA Select green fluorescent dye in PBS (Invitrogen). Cells were washed three times with PBS and mounted with Prolong Gold Antifade mounting medium with DAPI (Invitrogen).

Fluorescent i*n situ* hybridization (FISH).

The FISH protocol was performed as previously described [15]. Cells were fixed for 20 minutes at 4 ˚C in 4% PFA, 4% sucrose in PBS. RNA was precipitated by washing cells with 50% ethanol once, 100% ethanol once and rehydrated by washing once with 50% ethanol, and PBS twice. Cells were permeabilized and blocked for 30min in 3%BSA, 100mM glycine and 0.25% Triton X-100 (all from Thermo Fisher Scientific). For antigen retrieval cells were incubated for ten minutes with 1 ug/ml proteinase K (Thermo Fisher Scientific) at room temperature, washed three times with PBS, fixed for 10 minutes with 4% PFA 4%sucrose in PBS and washed three times for 5 minutes with 3% BSA, 100 mM glycine and 0.25% Triton X-100.

Cells were incubated with either 50 ng *Actb* or *Par3* targeting riboprobes labelled with digoxigenin in hybridization buffer containing 50% formamide (Sigma), 2X SSC (Sigma), 0.2% BSA, 1mg/ml *E.coli* tRNA (Sigma), 1mg/ml salmon sperm DNA (Fisher Scientific) for 3 hours and 30 minutes at 37 ºC. As a negative control green florescent protein targeting probes were used. Cells were washed with 50% formamide in 2X SSC once for 30 minutes at 37 ºC, once with 50% formamide in 1X SSC for 30 minutes at 37 ºC, three times with 1X SSC for 15 minutes each and three times with TBS containing 0.1% Tween at room temperature for 5 minutes each.

Samples were blocked and permeabilized for 30 minutes in 3% BSA, 0.1% Tween in TBS at room temperature and incubated overnight at 4 ºC with primary antibodies against digoxigenin (mouse monoclonal 1:500, Sigma) and β-actin (rabbit polyclonal 1:200, Sigma) in 3% BSA, 0.1% Tween in TBS. Cells were washed three times with TBS containing 0.1% Tween at room temperature for 5 minutes each and incubated

with the appropriate fluorophore-conjugated secondary antibodies for 1 hour at room temperature. Samples were washed with PBS twice for 5 minutes. Coverslips were airdried and mounted with Prolong Gold Antifade mounting medium with DAPI (Invitrogen, Thermo Fisher).

All the digoxigenin-conjugated riboprobes were synthetized with the T7 promoter (…GCCCTATAGTGAGTCGTATTAC-3') which were preceded by the following specific mRNA targeting sequences at the 3' end:

Actb.1: 5´-AACCGTGAAAAGATGACCCAGATCATGTTTGAGACCTTCAACACCCCAGC -3'.

Actb.2: 5´-ATGTGGATCAGCAAGCAGGAGTACGATGAGTCCGGCCCCTCCATCGTGCA -3'.

Actb.3: 5´-AGACCTCTATGCCAACACAGTGCTGTCTGGTGGCACCACCATGTACCCAG -3'.

Actb.4: 5´-GAGCGTGGCTACAGCTTCACCACCACAGCTGAGAGGGAAATCGTGCGTGA -3'.

Actb.5: 5´-TCCCTGGAGAAGAGCTATGAGCTGCCTGACGGTCAGGTCATCACTATCGG -3'.

Par3.1: 5'-GCCGTGCGGAGATGGCCGCATGAAAGTTTTCAGCCTTATCCAGCAGGCGG -3'.

Par3.2: 5'-TTCCACGAGAATGACTGCATTGTGAGGATTAACGATGGAGATCTTCGAAA -3'.

Par3.3: 5'-GGACGGTGGGATTCTAGACCTGGATGACATCCTCTGTGACGTTGCCGATG -3'.

Par3.4: 5'-TGCTTTTCGGCCTTATCAAACCACAAGTGAAATTGAGGTCACGCCTTCAG -3'.

Par3.5: 5'-TGCAGATTTGGGGATCTTCGTTAAGTCCATCATTAACGGGGGAGCTGCAT -3'.

Egfp.1: 5'-GATGCCACCTACGGCAAGCTGACCCTGAAGTTCATCTGCACCACCGGCAAG -3'.

Egfp.2: 5'-GACCACATGAAGCAGCACGACTTCTTCAAGTCCGCCATGCCCGAAGGCTAG -3'.

Egfp.3: 5'-ACTTCAAGGAGGACGGCAACATCCTGGGGCACAAGCTGGAGTACAACTACG -3'.

Egfp.4: 5'-AAGCAGAAGAACGGCATCAAGGTGAACTTCAAGATCCGCCACAACATCGAG -3'.

Egfp.5: 5'-AGTTCGTGACCGCCGCCGGGATCACTCTCGGCATGGACGAGCTGTACAAGG -3'.

The same FISH protocol was followed in mouse brain sections. After anaesthesia with 100mg/kg ketamine and 10mg/kg xylazine, 3-month-old mice (male and female) were transcardially perfused with NaCl 0.9%. Brains were removed and fixed in cold 4% PFA in PBS overnight at 4ºC. Samples were dehydrated first in 15% sucrose in PB 0.1M

and later in 30% sucrose in PB 0.1M, cryopreserved in OCT (Thermo Fisher Scientific), and 10 µm-think serial sagittal sections were obtained in a cryostat (Leica, Wetzlar, Germany). Sections were stored at -80 oC until used.

Puromycilation coupled with proximity ligation assays (PuroPLA).

Cells were treated with 250 ng/ml LPS (Sigma) or vehicle as previously described and exposed to 2µM puromycin (Sigma) for 2-10 minutes. Samples were fixed in 4% PFA and 4% sucrose in PBS, washed three times with PBS for 5 minutes and permeabilized and blocked for 30 min in 3% BSA, 100 mM glycine and 0.25% Triton X-100 (all from Thermo Fisher Scientific). Cells were incubated overnight at 4 ^{o}C with an anti-puromycin antibody (mouse monoclonal 1:500, Merck) combined with an anti-β-actin antibody (rabbit polyclonal 1:1000, 07-Sigma) or an anti-Par3 antibody (rabbit polyclonal 1:200, Sigma). Detection of newly synthesized β-actin or Par3 through PuroPLA was performed according to the manufacturer's instructions, using rabbit PLAplus and mouse PLAminus probes and red Duolink detection reagents (Sigma Aldrich). Before mounting with Duolink *in situ* mounting medium with DAPI (Sigma Aldrich), coverslips were incubated with Alexa Fluor488-conjugated phalloidin (1:800; Thermo Fisher Scientific) for 30 minutes at room temperature.

***Imp1* knockdown experiments.**

Imp1 genetic silencing was performed using small interference RNAs (siRNA) in serum-free medium in the absence of antibiotics. Double stranded siRNAs were transfected with lipofectamine RNA iMAX (Invitrogen, Thermo Fisher) following manufacturer recommendations. Cells were transfected for 6 or 24 hours with Imp1-targeting siRNAs (siRNA #1: s155193, or siRNA #2: s155193. Both from Ambion, Thermo Fisher Scientific).

The sequences of *Imp1*-targeting siRNAs are the following:

siRNA #1: 5' – GGAAAAUACAGAUCCGGAAtt – 3'

siRNA #2: 5' – GCCUGAGAAUGAGUGGGAAtt – 3'

Transfection efficiency was analyzed by immunocytochemistry with an anti-IMP1/ZBP1 antibody (mouse monoclonal 1:500, MBL).

Migration assays.

Microglia were obtained from a mixed glial culture as previously described. Cells (60.000-80.000 cells/cm^2) were seeded in a transwell system which consists of a culture insert with a polyethylene terephthalate membrane that creates two compartments. Cells were seeded onto PDL-coated membranes with 3 µm-pores which enabled microglial migration toward the lower compartment, or with 1 µm- pores in which cell body migration was restricted. The lower compartment was treated with 150 ng/ml LPS or PBS for 30 minutes. Migration of the nuclei and the cytoskeleton were addressed by DAPI and phalloidin staining respectively.

Phagocytosis.

The protocol for *in vitro* phagocytosis was adapted from Beccari and colleagues [31]. Briefly, SH-SY5Y cell lines stably transfected with the red fluorophore tFP602 (SH-SY5Y vampire. InnoProt, Derio, Spain) were cultured in DMEM (Gibco, Thermo Fisher Scientific) containing 10% fetal bovine serum (Sigma Aldrich), 10% penicillin/streptomycin/glutamine (Gibco, Thermo Fisher Scientific) and 250 µg/ml

geneticin (Gibco, Thermo Fisher Scientific). Apoptosis was induced by adding 3 µM staurosporine (Sigma Aldrich) for 4 hours at 37 ^{o}C. The medium was collected and centrifuged for 4 minutes at 1300 rpm. Apoptotic cells were resuspended microglia plating medium and added to microglial primary cultures in a 1:3 ratio (SH-SY5Y:microglia) for 1 hour before fixation and processing. Primary microglia were exposed to LPS or vehicle for 30 minutes prior to adding the apoptotic cells. Phagocytosis was addressed by quantifying the percentage of phalloidin-labelled microglia containing vampire particles as well as the particle size.

Image acquisition.

Images were acquired using an EC Plan-Neofluar 40×/1,30 Oil DIC M27 objective on an Axio-Observer Z1 microscope equipped with AxioCam MRm Rev. 3 (Zeiss, Oberkochen, Germany) and Hamamatsu EM-CCD ImagEM (Hamamatsu Photonics, Hamamatsu, Japan) digital cameras. Settings for image acquisition of cultured microglia were determined in a random field of a control sample ensuring pixel intensities were within the linear range and avoiding pixel saturation. Images were acquired with ZEN 2 (blue edition) version 2.0.0.0. software (Zeiss). Cells were selected based on the counterstain (e.g phalloidin) for the blind acquisition of the labelling of interest and settings were kept identical for all sampled cells in any given experiment. Whenever possible, five random fields per coverslip and two coverslips per experimental condition were imaged. In the case of microglia sampled from mouse brains, individual Iba1-positive cells were randomly imaged from the polymorphic cell layer of the dentate gyrus of 10 µm-thick brain sagittal sections. 6 stacks were imaged per field using structured illumination with Apotome2 (Zeiss) and the summed mean pixel intensity was used for quantification.

For presentation in figures the greyscale images were converted to RGB and contrast and background settings were set the same in control and experimental conditions for the staining of interest. Markers used as counterstain for MPP selection were adjusted for an optimal visualization in figures.

Fluorescence quantification.

Fluorescence intensity for the staining of interest was measured in random cells in FIJI/ImageJ (NIH, Bethesda, MD, USA). Concentric circles of 5 µm or 2 µm intervals emerging from the edge of the soma or from the nucleus were generated by an in-house designed FIJI/ImageJ macro and the intensity was measured in each bin as previously described [21] and averaged. Background fluorescence was measured outside the cell and substracted.

SYTO-, FISH- and IMP1/ZBP1-positive foci were measured on binarized images as previously described [21]. The number of objects was scored for each staining in MPPs or the soma with the Analyze Particle function in FIJI/ImageJ (NIH) and normalized to area or MPP length. Given the discrete numbers of Puro-PLA puncta these were manually quantified on raw images.

Statistical analysis.

The sample size is specified in the figure legends. Statistical analyses were performed with Prism 8 and 10 (GraphPad Software, San Diego, CA, United States) following a randomized block design where samples from the same experiment were matched to eliminate inter-experimental variability. Unless otherwise stated, when comparing the means of two groups taking one variable into account, two-tailed t-tests were

performed. One-way ANOVA followed by Holm-Sidak´s multiple comparison test was used if one variable was compared between more than two groups. If more than one variable was analyzed, we performed two-way ANOVA followed by Holm Sidak's multiple comparison test.

REFERENCES

1 Jung, H., Gkogkas, C. G., Sonenberg, N. & Holt, C. E. Remote control of gene function by local translation. *Cell* **157**, 26-40, doi:10.1016/j.cell.2014.03.005 (2014).

2 Martin, K. C. & Ephrussi, A. mRNA localization: gene expression in the spatial dimension. *Cell* **136**, 719-730, doi:10.1016/j.cell.2009.01.044 (2009).

3 Jung, H., Yoon, B. C. & Holt, C. E. Axonal mRNA localization and local protein synthesis in nervous system assembly, maintenance and repair. *Nat Rev Neurosci* **13**, 308-324, doi:10.1038/nrn3210 (2012).

4 Batista, A. F. R., Martinez, J. C. & Hengst, U. Intra-axonal Synthesis of SNAP25 Is Required for the Formation of Presynaptic Terminals. *Cell Rep* **20**, 3085-3098, doi:10.1016/j.celrep.2017.08.097 (2017).

5 Sun, C. *et al.* The prevalence and specificity of local protein synthesis during neuronal synaptic plasticity. *Sci Adv* **7**, eabj0790, doi:10.1126/sciadv.abj0790 (2021).

6 Blanco-Urrejola, M. *et al.* RNA Localization and Local Translation in Glia in Neurological and Neurodegenerative Diseases: Lessons from Neurons. *Cells* **10**, 632 (2021).

7 Oudart, M. *et al.* AstroDot - a new method for studying the spatial distribution of mRNA in astrocytes. *J Cell Sci* **133**, doi:10.1242/jcs.239756 (2020).

8 Vasek, M. J. *et al.* Local translation in microglial processes is required for efficient phagocytosis. *Nat Neurosci*, doi:10.1038/s41593-023-01353-0 (2023).

9 Nimmerjahn, A., Kirchhoff, F. & Helmchen, F. Resting microglial cells are highly dynamic surveillants of brain parenchyma in vivo. *Science* **308**, 1314-1318, doi:10.1126/science.1110647 (2005).

10 Franco-Bocanegra, D. K., McAuley, C., Nicoll, J. A. R. & Boche, D. Molecular Mechanisms of Microglial Motility: Changes in Ageing and Alzheimer's Disease. *Cells* **8**, doi:10.3390/cells8060639 (2019).

11 Kettenmann, H., Hanisch, U. K., Noda, M. & Verkhratsky, A. Physiology of microglia. *Physiol Rev* **91**, 461-553, doi:10.1152/physrev.00011.2010 (2011).

12 Bernier, L. P. *et al.* Nanoscale Surveillance of the Brain by Microglia via cAMP-Regulated Filopodia. *Cell Rep* **27**, 2895-2908 e2894, doi:10.1016/j.celrep.2019.05.010 (2019).

13 Bridgman, P. C. & Dailey, M. E. The organization of myosin and actin in rapid frozen nerve growth cones. *J Cell Biol* **108**, 95-109, doi:10.1083/jcb.108.1.95 (1989).

14 Kislauskis, E. H., Zhu, X. & Singer, R. H. beta-Actin messenger RNA localization and protein synthesis augment cell motility. *J Cell Biol* **136**, 1263-1270, doi:10.1083/jcb.136.6.1263 (1997).

15 Hengst, U., Deglincerti, A., Kim, H. J., Jeon, N. L. & Jaffrey, S. R. Axonal elongation triggered by stimulus-induced local translation of a polarity complex protein. *Nat Cell Biol* **11**, 1024-1030, doi:10.1038/ncb1916 (2009).

16 Ross, A. F., Oleynikov, Y., Kislauskis, E. H., Taneja, K. L. & Singer, R. H. Characterization of a beta-actin mRNA zipcode-binding protein. *Mol Cell Biol* **17**, 2158-2165, doi:10.1128/MCB.17.4.2158 (1997).

17 Perycz, M., Urbanska, A. S., Krawczyk, P. S., Parobczak, K. & Jaworski, J. Zipcode binding protein 1 regulates the development of dendritic arbors in hippocampal neurons. *J Neurosci* **31**, 5271-5285, doi:10.1523/JNEUROSCI.2387-10.2011 (2011).

18 Donnelly, C. J. *et al.* Limited availability of ZBP1 restricts axonal mRNA localization and nerve regeneration capacity. *EMBO J* **30**, 4665-4677, doi:10.1038/emboj.2011.347 (2011).
19 Nunez, L. *et al.* Tagged actin mRNA dysregulation in IGF2BP1[Formula: see text] mice. *Proc Natl Acad Sci U S A* **119**, e2208465119, doi:10.1073/pnas.2208465119 (2022).
20 Schmidt, E. K., Clavarino, G., Ceppi, M. & Pierre, P. SUnSET, a nonradioactive method to monitor protein synthesis. *Nat Methods* **6**, 275-277, doi:10.1038/nmeth.1314 (2009).
21 Gamarra, M., Blanco-Urrejola, M., Batista, A. F. R., Imaz, J. & Baleriola, J. Object-Based Analyses in FIJI/ImageJ to Measure Local RNA Translation Sites in Neurites in Response to Abeta1-42 Oligomers. *Front Neurosci* **14**, 547, doi:10.3389/fnins.2020.00547 (2020).
22 Sierra, A. *et al.* Microglia shape adult hippocampal neurogenesis through apoptosis-coupled phagocytosis. *Cell Stem Cell* **7**, 483-495, doi:10.1016/j.stem.2010.08.014 (2010).
23 Savas, J. N. *et al.* A role for huntington disease protein in dendritic RNA granules. *J Biol Chem* **285**, 13142-13153, doi:10.1074/jbc.M110.114561 (2010).
24 Leung, K. M. *et al.* Asymmetrical beta-actin mRNA translation in growth cones mediates attractive turning to netrin-1. *Nat Neurosci* **9**, 1247-1256, doi:10.1038/nn1775 (2006).
25 tom Dieck, S. *et al.* Direct visualization of newly synthesized target proteins in situ. *Nat Methods* **12**, 411-414, doi:10.1038/nmeth.3319 (2015).
26 Triantopoulou, N. & Vidaki, M. Local mRNA translation and cytoskeletal reorganization: Mechanisms that tune neuronal responses. *Front Mol Neurosci* **15**, 949096, doi:10.3389/fnmol.2022.949096 (2022).
27 Walker, C. A. *et al.* Abeta1-42 triggers the generation of a retrograde signaling complex from sentinel mRNAs in axons. *EMBO Rep* **19**, doi:10.15252/embr.201745435 (2018).
28 Tushev, G. *et al.* Alternative 3' UTRs Modify the Localization, Regulatory Potential, Stability, and Plasticity of mRNAs in Neuronal Compartments. *Neuron* **98**, 495-511 e496, doi:10.1016/j.neuron.2018.03.030 (2018).
29 Pintacuda, G. *et al.* Protein interaction studies in human induced neurons indicate convergent biology underlying autism spectrum disorders. *Cell Genom* **3**, 100250, doi:10.1016/j.xgen.2022.100250 (2023).
30 Lin, R. *et al.* Directed evolution of adeno-associated virus for efficient gene delivery to microglia. *Nat Methods* **19**, 976-985, doi:10.1038/s41592-022-01547-7 (2022).
31 Beccari, S., Diaz-Aparicio, I. & Sierra, A. Quantifying Microglial Phagocytosis of Apoptotic Cells in the Brain in Health and Disease. *Curr Protoc Immunol* **122**, e49, doi:10.1002/cpim.49 (2018).

ACKNOWLEDGEMENTS

We thank Dr. Mariana Astiz for critical review of our manuscript and for her suggestions to improve our work.

FUNDING

This work was supported by two grants from the Spanish Ministry of Science and Innovation (RYC-2016-19837 and PID2019-110721RB-I00) and start-up funds from the Basque Foundation for Science (IKERBASQUE) to JB. JI-I and AdC-G are predoctoral fellows funded by the Basque Government. MB-U is a predoctoral fellow funded by the University of the Basque Country (UPV/EHU).

AUTHOR CONTRIBUTIONS

JB conceived the project and designed the experiments together with JI-I and MB-U. JI-I, MB-U and AdC-G performed and analyzed the experiments. MM and AS assisted with phagocytosis assays a prepared SH-SY5Y vampire neuronal cell lines. JB and JI-I drafted the manuscript and prepared the figures. JB, JI-I and AS edited the manuscript.

DATA AVAILABILITY

The datasets generated for this study are available on request to the corresponding author.

CONFLICT OF INTEREST

The authors declare no conflict of interests.

SUPPLEMANTARY MATERIAL

Supplementary figure 1

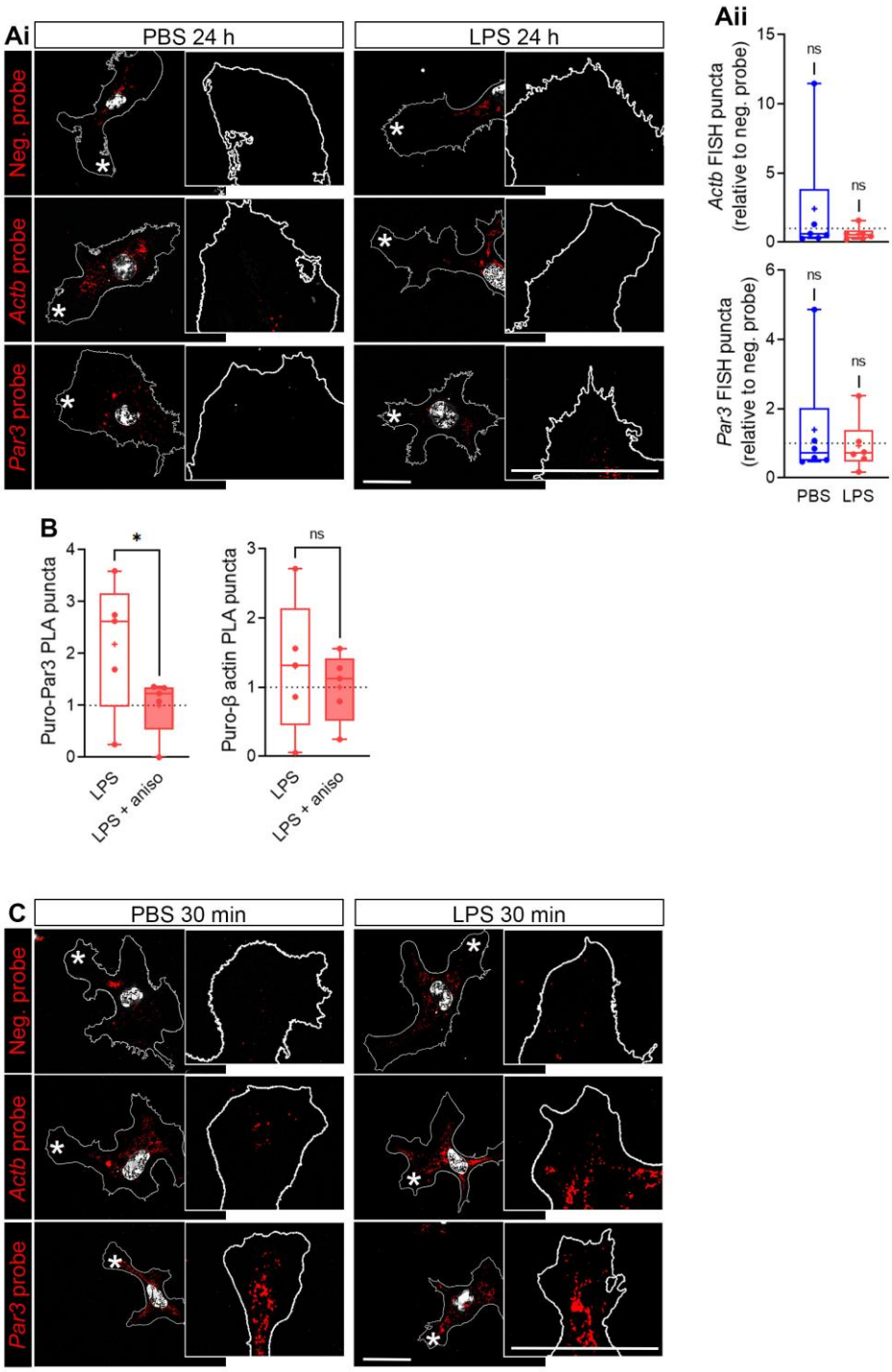

Supplementary figure 1- *Actb* and *Par3* mRNA levels and their localized translation in microglia upon LPS exposure. (A) A prerequisite for localized translation is the presence of mRNAs in cell peripheral structures. We addressed the localization of *Actb* and *Par3* mRNAs to microglial lamella by fluorescent *in situ* hybridization (FISH) and did not observe any positive signal compared to a negative when cells were exposed to PBS or LPS for 24 hours. Representative images of FISH are shown in (A^i). Scale bar, 20 µm. Asterisks indicate the lamellae shown in insets. Box and whisker plots indicate the number of *Actb* (A^{ii}, upper graph) and *Par3* (A^{ii}, lower graph) mRNA foci relative to the negative probe quantified in 6 independent

experiments (n=6). One-way ANOVA followed by Dunnet´s multiple comparison test. ns, not significant; **(B)** Translation of *Par3*, but not of *Actb*, is detected in microglial lamellae upon exposure to LPS for 24 hours. Translation of *Actb* and *Par3* was assessed with a 10-minute puromycin pulse in LPS-treated cells followed by proximity ligation assay (PLA) with antibodies against puromycin and β actin, and against puromycin and Par3 respectively. Graphs represent the average PLA puncta quantified in LPS-treated cells preincubated with vehicle or anisomycin in 5 independent experiments (n=5) analyzed by two-tailed t tests. *$p < 0.05$; ns, not significant. **(C)** Detection of *Actb* and *Par3* mRNAs in the periphery of microglia by FISH after exposure to PBS or LPS for 30 minutes. Scale bar, 20 µm. Asterisks indicate the lamellae shown in insets.

Supplementary figure 2

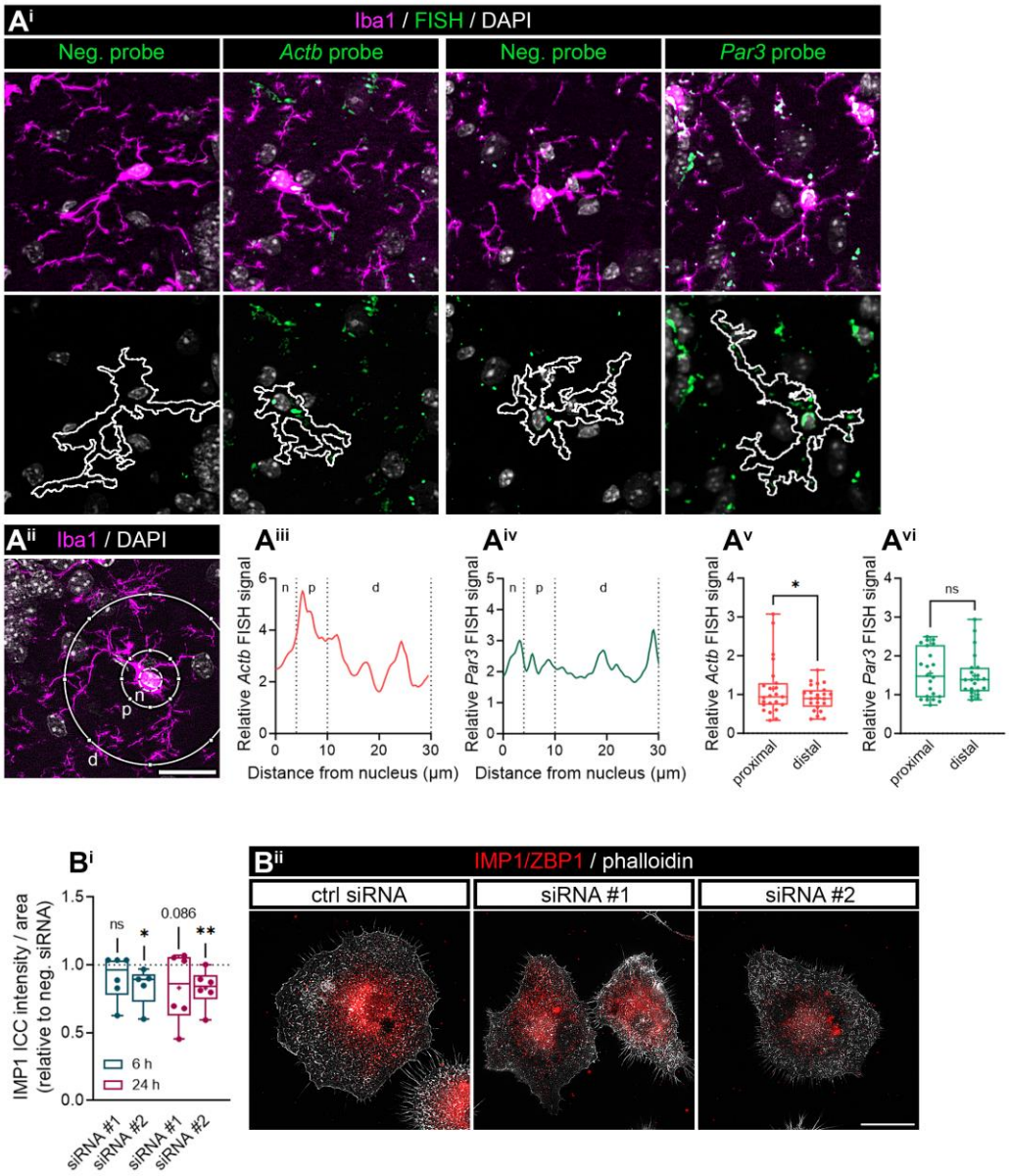

Supplementary figure 2- *Actb* and *Par3* distribution in microglia of the dentate gyrus in 3-month-old animals and downregulation of RNA binding protein IMP1/ZBP1 with targeting siRNAs. (A) *Actb* and *Par3* distribution in the polymorphic cell layer of the dentate gyrus in 3-month-old mice compared to a non-targeting probe (A^{i}). *Actb* and *Par3* relative levels were measured in the nucleus (n) in proximal (p) and in distal (d) MPPs as specified in (A^{ii}). Relative distribution of *Actb* and *Par3* are exemplified (A^{iii} and A^{iv}). The box and whisker plots represent the relative levels of *Actb* (A^{v}) and *Par3* (A^{vi}) in proximal and distal microglial processes measured by FISH in 22-23 microglial cells (4 independent mice). Two-tailed t tests was performed. *$p < 0.05$; n.s, not significant. Scale bar, 20 µm. **(B)** Knockdown efficiency of two nonoverlapping siRNAs targeting *Imp1* compared to a negative siRNA following 6 and 24 hours of transfection. The box and whisker graph represents the mean intensity of IMP1 protein in

cells transfected with a control siRNAs and two *Imp1* siRNAs from 5-6 independent experiments (n=5-6). Two-tailed t tests was performed, *$p < 0.05$; **$p < 0.01$; n.s, not significant, siRNA #1 vs ctrl siRNA (dashed line) and siRNA #2 vs ctrl siRNA (dashed line) (B^{i}). Representative micrographs of transfected cells are shown. Scale bar, 20 µm (B^{ii}).

Supplementary figure 3

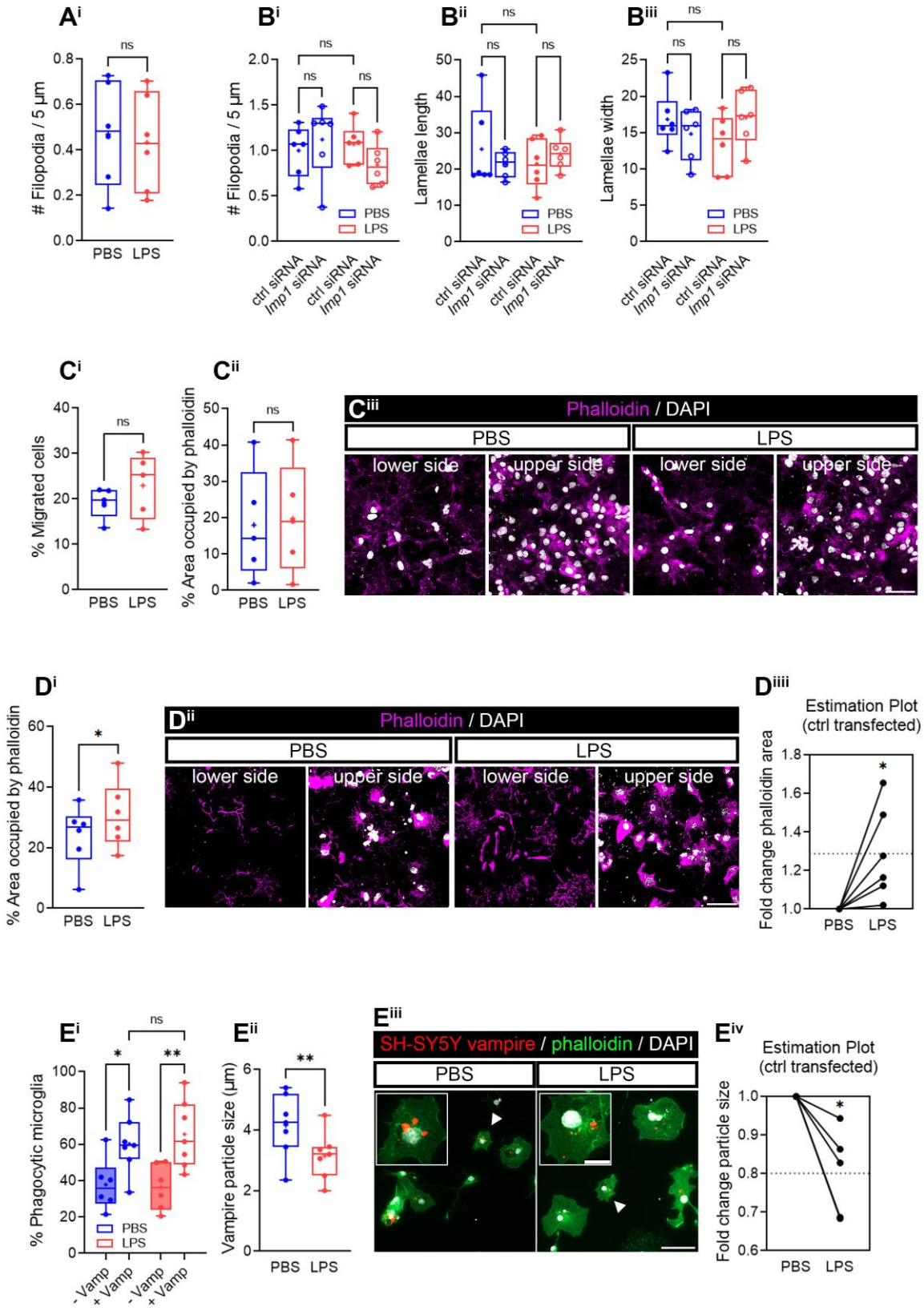

Supplementary figure 3- Effect of acute LPS exposure on the number of filopodia lamellar morphology, migration and phagocytosis. (A) Number of filopodia in PBS- and LPS-treated microglia. The box and whisker plot represents the results form 6 independent experiments (n=6). Two-tailed t test was performed, n.s; not significant. **(B)** Number of filopodia (B^{i}), lamellar length (B^{ii}) and width (B^{iii}) in cells transfected with control (ctrl KD) or *Imp1* siRNA (*Imp1* KD) and exposed to PBS or LPS for 30 minutes. The box and whisker plots represent the results form 6 independent experiments (n=6). One-way ANOVA followed by Holm-Šídák's multiple comparison test was performed, n.s; not significant.. **(C)** Microglial migration in a 3 µm-pore transwell culture system. Migration was first analyzed as the percentage of microglial nuclei (DAPI) found in the lower side of the chamber with respect to the total nuclei (DAPI) found in both the upper and lower chambers (C^{i}). The area covered by phalloidin in the lower compartment was also measured to assess F-actin-rich cytoskeleton extension (C^{ii}). Both box and whisker plots represent the results from 5 independent experiments (n=5). Two-tailed t testwas performed, n.s; not significant. Representative micrographs of nuclear (DAPI) and F-actin (phalloidin) staining in the lower and upper compartments of transwells is shown. Scale bar, 100 µm (C^{iii}). **(D)** Microglial migration in a 1 µm-pore transwell culture system. Somatic migration was restricted in this culture setup, and only MPPs were observed in the lower chamber. We treated the lower compartment and assessed polarized microglial MPP migration by the area covered by phalloidin in the lower compartment in PBS- and LPS-treated cells. Box and whisker graph represents F-actin-rich cytoskeleton extension (phalloidin staining) measured in 6 independent experiments (n=6). Two tailed t test was performed, $*p < 0.05$ (D^{i}). Micrographs depicting nuclear migration (DAPI) and F-actin extension (phalloidin) toward the lower compartment are shown. Scale bar, 100 µm (D^{ii}). LPS effect on cytoskeleton extension was addressed in control- (ctrl) transfected cells to determine the reproducibility of our results compared to those in untransfected cells. Despite the variability mentioned in the main text, we did observe a consistent relative effect on polarized MPP migration in LPS- compared to PBS-treated cells. Two tailed t test was performed, $p^{*}< 0.05$, (D^{ii}). **(E)** Percentage of phagocytic microglia and size of phagocytosed particles in response to LPS. Cultured microglia were fed with human SH-SY5Y apoptotic neurons labelled with vampire, previously treated with PBS or LPS for 30 minutes. The percentage of microglia with vampire-positive particles inside was quantified (+Vamp) compared to a negative control (-Vamp). Box and whisker graphs from 7 independent experiments (n=7) show no differences in phagocytic microglia in PBS or LPS treatments (E^{i}). However, particles were smaller in LPS-treated cells compared to controls as represented from the box and whisker plots from 7 independent experiments (n=7). Two tailed t test was performed, $**p < 0.01$ (E^{ii}). Vampire particle size in PBS- and LPS-treated microglia is shown in representative micrographs (E^{iii}). LPS effect on vampire particle sized was addressed in control- (ctrl) transfected cells to determine the reproducibility of our results compared to those in untransfected cells. Despite the variability mentioned in the main text, we did observe a consistent relative effect on the size of vampire particles in phagocytic microglia in LPS-compared to PBS-treated cells. Two tailed t test was performed, $*p < 0.05$, (E^{iv}).